Laser and Particle Beams (2015), *33*, 315–330.

doi:10.1017/S0263034615000312

Effect of nature and pressure of ambient environments on the surface morphology, plasma parameters, hardness, and corrosion resistance of laser-irradiated Mg-alloy

ASADULLAH DAWOOD, SHAZIA BASHIR, MAHREEN AKRAM, ASMA HAYAT, SAJJAD AHMED, MUHAMMAD HASSAN IQBAL, AND ALI HASSAN KAZMI

Centre for Advanced Studies in Physics (CASP), Government College University Lahore, Lahore, Pakistan

(RECEIVED 12 December 2014; ACCEPTED 20 February 2015)

Abstract

The influence of nature and pressure of ambient environment on the surface modification, plasma parameters, hardness, and corrosion resistance of Mg-alloy has been investigated. Nd: YAG laser (1064 nm, 10 ns, 25 mJ) at a fluence of 1.3 J cm^{-2} has been employed as an irradiation source. Targets of Mg-alloy were exposed in the ambient environments of argon (Ar), neon (Ne), and helium (He) at pressures ranging from 5 to 760 Torr. Scanning electron microscope has been employed to investigate the surface morphology of the irradiated targets. It reveals the formation of cavities, cones, droplets, ripples, and islands on the surface of the irradiated sample. Laser-induced breakdown spectroscopy technique was employed to measure electron temperature (T_e) and electron number density (N_e) of Mg-alloy. The value of electron temperature ranges from 6628 to 12,855 K, whereas the value of electron number density varies from 5.4×10^{17} to 19.2×10^{17} cm^{-3}. The maximum T_e and N_e are observed in Ar and minimum in case of He. It was also revealed that both the surface morphology and plasma parameters are strongly dependent upon nature and pressure of environmental gases. The maxima of T_e is achieved at a pressure of 10 Torr for all the three ambient environments that is, Ar, Ne, and He; whereas maxima of N_e is achieved at different pressures, that is, at 760 Torr for Ar, at 200 Torr for Ne, and at 50 Torr for He. The hardness and corrosion resistance of irradiated Mg-alloy have been explored using Vickers Micro-hardness tester and Potentio-dynamic polarization technique, respectively. It was investigated that as compared with un-irradiated target, the hardness as well as corrosion resistance of the laser-irradiated target has been increased significantly in all environments. Plasma parameters, mechanical, and electrical properties of laser-irradiated Mg-alloy have been correlated with induced surface modifications and are strongly influenced by environmental conditions.

Keywords: Electron density; Electron temperature; Laser-induced breakdown spectroscopy; Mg-alloy; Surface structuring

1. INTRODUCTION

Laser ablation of materials is an emerging technique with wide range of applications in the field of Physics, Chemistry, material science, medicine, agriculture, and industry (Phipps, 2007). Laser-assisted ablation, deposition, and plasma parameters are influenced by various parameters such as laser fluence, environmental conditions, and material properties. It is reported that plasma parameters play a significant role for micro/nano-structuring of material. Different physical processes such as confinement effect, shielding effect, formation of shock waves, clustering, and interaction of plasma plume with ambient gas are strongly influenced by the environmental conditions (Hafeez *et al*., 2008; Farid *et al*., 2012).

Laser-induced breakdown spectroscopy (LIBS) is a beneficial technique for many applications such as analysis of metals, aerosols, soils, coal quality, cultural heritage, and forensics (Diwakar, 2014; Gondal & Dastageer, 2014; Legnaioli *et al*., 2014). It can also be used as geochemical finger printing, space exploration, and biomedical applications (Cremers, 2014; Hark & Harmon 2014; Legnaioli *et al*., 2014; Moros *et al*., 2014). It is a simplest technique in which a focused laser beam is used as an excitation source to

Address correspondence and reprint requests to: Shazia Bashir, Centre for Advanced Studies in Physics (CASP), Government College University Lahore, Katchery Rd, Lahore 54000, Pakistan. E-mail: shaziabashir@gcu.edu.pk

generate high-temperature and high-density plasma. Two processes such as multi-photon ionization and inverse bremsstrahlung ionization are responsible for the generation and cascade growth of electrons as well as high-density and high-temperature plasma. Photons emission due to de-excitation and recombination of electrons with ions is examined by a high-resolution spectrometer (Khan *et al*., 2013).

LIBS system is an adequate tool for plasma characterization. Many research groups have investigated the effect of nature and pressure of background gases on surface structuring, plasma parameters, and hardness (Harilal *et al*., 1998*a*; 1998*b*; Hafeez *et al*., 2008; Farid *et al*., 2012; Nakimana *et al*., 2012).

Mg-alloy with commercial name AZ31B is selected for the present investigation due to its good room-temperature strength, ductility, corrosion resistance, and weldability. Nowadays, this alloy is widely applicable in auto and electronics industry (computer, communication, and consumer electronics). It is useful for the coating of mobile phones, cars, and air planes. Laser irradiation can improve its physical properties, for example, hardness, corrosion resistance, and bio-compatibility. By laser treatment the improvement in the corrosion resistance is by many research groups.

Majumdar *et al*. (2003) investigated the effect of laser irradiation on corrosion and wear resistance of a commercial Mg-alloy. Result of their investigation depicted that micro-hardness, corrosion resistance, and wear resistance of the laser surface melted layer was improved as compared with as-received Mg-alloy. Khalfaoui *et al*. (2010) studied laser surface melting treatment performed on a ZE41 Mg-alloy using an excimer KrF laser. Their investigation depicted that laser treatment increased the micro-hardness of the ZE41 Mg-alloy and improved its corrosion resistance.

Many research groups have investigated the effect of ambient environment and pressure on the growth of surface structures, and plasma parameters (Warcholinski & Gilewicz, 2009; Nakimana *et al*., 2012; Salik *et al*., 2014). Salik *et al*. (2014) investigated the effect of different wavelengths of a *Q*-switched Nd: YAG laser on plasma parameters of manganese sulfate at different ambient air pressures and with laser irradiance. Their investigation revealed that electron temperature calculated for 1064 nm was higher than 532 nm. On the other hand, the electron number density was reported higher for 532 nm as compared with 1064 nm. Farid *et al*. (2012) investigated that Cu plasma characteristics and surface morphology were strongly influenced by the nature and pressure of ambient environment of argon (Ar), neon (Ne), and helium (He) at 200 mJ. The purpose of their investigation was to improve experimental conditions for pulsed laser deposition of thin films and nano-structuring of target material.

Nakimana *et al*. (2012) investigated that environmental gas pressure is one of the controlling factor for plasma plume characteristics. Their measurements depicted that some lines which are nearly unresolved at high pressures become well resolved at low pressures.

According to our best knowledge no work is reported in which the effect of ambient environment and pressure on surface structures of Mg-alloy, plasma parameters, hardness, and corrosion resistance has been investigated.

In the present work, laser ablation of Mg-alloy has been performed at different pressures ranging from 5 to 760 Torr under ambient environments of Ar, Ne and He. Scanning electron microscope (SEM) analysis has been performed to investigate the surface modification of irradiated target at different pressures. LIBS technique has been employed to investigate plasma parameters such as emission intensity, electron temperature, and electron number density of Mg-alloy. Electron temperature is calculated by the Boltzmann plot method. Stark broadening mechanism is employed for the calculation of electron number density. The micro-hardness of irradiated target was investigated by Vickers hardness tester. The corrosion resistance of treated sample was studied by Potentiostat.

The purpose of the present work is to find out the optimum conditions of plasma parameters which are favorable for the growth of surface structures. The aim of the work is to identify the optimal condition for the improvement of mechanical and electrical properties such as hardness and corrosion resistance of the irradiated Mg-alloy.

2. EXPERIMENTAL SETUP

Squared Mg-alloy samples with dimensions of $20 \times 20 \times 5\ mm^3$ were used as target. The chemical composition of Mg-alloy is given in Table 1. Samples were mechanically grinded, polished, and then ultrasonically cleaned for 20 min to remove contamination before laser ablation. Targets were mounted on sample holder in a stainless steel vacuum chamber. Figure 1 depicts the schematic of the experimental setup.

To perform ablation and emission spectroscopy of Mg-alloy, Nd: YAG laser (CRF200: Big Sky Laser Technologies, Quantel, France) with wavelength of 1064 nm, pulse duration of 10 ns, pulse energy of 25–400 mJ, with a repetition rate of 1–10 Hz has been used as an irradiation source. The laser beam was focused through a lens of focal length

Table 1. *Chemical composition of Mg-alloy used as a target material*

Element	Content (%)
Magnesium (Mg)	97
Aluminum (Al)	2.50–3.50
Zinc (Zn)	0.60–1.40
Manganese (Mn)	0.20
Silicon (Si)	0.10
Copper Cu)	0.050
Calcium (Ca)	0.040
Iron (Fe)	0.0050
Nickel (Ni)	0.0050

https://doi.org/10.1017/S0263034615000312 Published online by Cambridge University Press

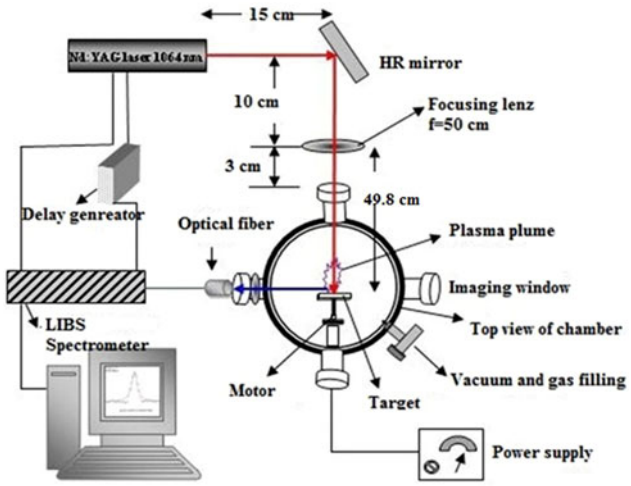

Fig. 1. The schematic of the experimental setup for ablation and emission spectroscopy of Mg-alloy by employing Nd: YAG laser as a source of excitation.

50 cm and was incident at an angle of 90° with respect to target surface. Mg-alloy samples were irradiated at a distance of 49.8 cm (from focusing lens) before the focus. The purpose of this pre-focus arrangement is to minimize relevant gas breakdown. The focused spot size of Mg-alloy comes out to be 1.9×10^{-2} cm^2. Spectrometer system (LIBS 2500 plus) is employed for analysis of emission spectra having a wavelength range 200–980 nm, resolution 0.1 nm. These data are collected by optical fiber which was placed outside of the vacuum chamber and the distance between the optical fiber and the surface of the specimen is 9 cm. The emission spectra are transmitted through quartz window placed at side port of vacuum chamber. Then the signal was sent to the focusing lens of focal length of 5 cm and diameter of 2 cm placed outside of vacuum chamber. This lens is used to converge and amplify the signal which is then sent to the optical fiber placed at a distance of 5 cm from the converging lens.

Two sets of experiments were carried out:

1. For SEM analysis first set of experiment was performed at the three environments of gases such as Ar, Ne, and He. These gases were filled at a pressure of 5, 50, 300, and 760 Torr in chamber turn by turn and their pressure was measured by precised pressure gauge. Mg-alloy was irradiated for 200 laser pulses at pulse energy 25 mJ corresponding to laser fluence of 1.3 J cm^{-2}.
2. The second set of experiment was performed for the LIBS analysis. In this set of experiment 11 targets were exposed by single laser pulse at constant pulse energy of 25 mJ and at a fluence of 1.3 J cm^{-2}. The three environmental gases of Ar, Ne, and He were filled at 11 various pressures of 5, 10, 20, 50, 100, 200, 300, 400, 500, 600, and 760 Torr. The emission spectra were collected for each process using optical fiber cable connected to the LIBS spectrometer.

The surface structuring of the irradiated specimens were examined using SEM (JEOL JSM 6490-A). Micro-hardness of irradiated target was investigated by micro-hardness tester (Zwick/Roell ZHV 5030). The corrosion resistance of irradiated target was examined by Potentiostat (PC14/750).

3. RESULTS AND DISCUSSION

3.1. Effect of Ambient Environment and its Pressure on the Surface Morphology

SEM micrographs of Figures 2a–2d represent centrally ablated area of Mg-alloy under Ar environment after irradiation at a fluence of 1.3 J cm^{-2} for different pressures of (a) 5, (b) 50, (c) 300, and (d) 760 Torr. From Figure 2a it is observed that by treating the sample for the lowest gas pressure of 5 Torr cones and diffused ripples are observed. It was noticed that cones and ripples are completely merged by increasing the pressure from 5 Torr (Fig. 2a) to 50 Torr (Fig. 2b). By increasing pressure from 300 Torr (Fig. 2c) to 760 Torr (Fig. 2d) cone formation is seen with an appearance of splashed surface. In addition to other features, droplets are also observed as shown in Figures 2b–2d. The density of droplets decreases and size increases with increasing pressure as the pressure is increased from 300 to 760 Torr. Figure 2d reveals that for the highest pressure of 760 Torr, splashing and melting is enhanced.

The SEM micrographs of Figures 3a–3d represent peripheral ablated area of Mg-alloy under Ar environment after irradiation at a fluence of 1.3 J cm^{-2} for different pressures of (a) 5, (b) 50, (c) 300, and (d) 760 Torr. For the lowest pressure micro-sized cavities and cones with high-scale melting are observed as shown in Figure 3a. Figure 3b shows that the size and density of micro-sized cavities is reduced at a pressure of 50 Torr and ablative layers are grown along the periphery of cavities. Figure 3c shows the formation of large size cones after irradiation at a pressure of 300 Torr, whereas cavities and droplets have completely wiped out. Figure 3d shows that more distinct and large-sized cones are formed for the maximum pressures of 760 Torr.

The SEM micrographs of Figures 4a–4d show centrally ablated area of Mg-alloy under Ne environment after irradiation at a fluence of 1.3 J cm^{-2} for different pressures of (a) 5, (b) 50, (c) 300, and (d) 760 Torr. For the lowest pressure 5 Torr ripples and large density of cones are observed as shown in Figure 4a. Figure 4b illustrates the appearance of wavy-like structures at a pressure of 50 Torr. Figure 4c depicts the droplet formation at 300 Torr. Redeposition of ejected material is also observed in Figure 4c. Figure 4d displays the distinct cones, droplets along large-scale melting for the maximum pressures of 760 Torr.

The SEM micrographs of Figures 5a–5d show peripheral ablated area of Mg-alloy under Ne environment after irradiation at a fluence of 1.3 J cm^{-2} for different pressures of (a) 5, (b) 50, (c) 300, and (d) 760 Torr. For the lowest

https://doi.org/10.1017/S0263034615000312 Published online by Cambridge University Press

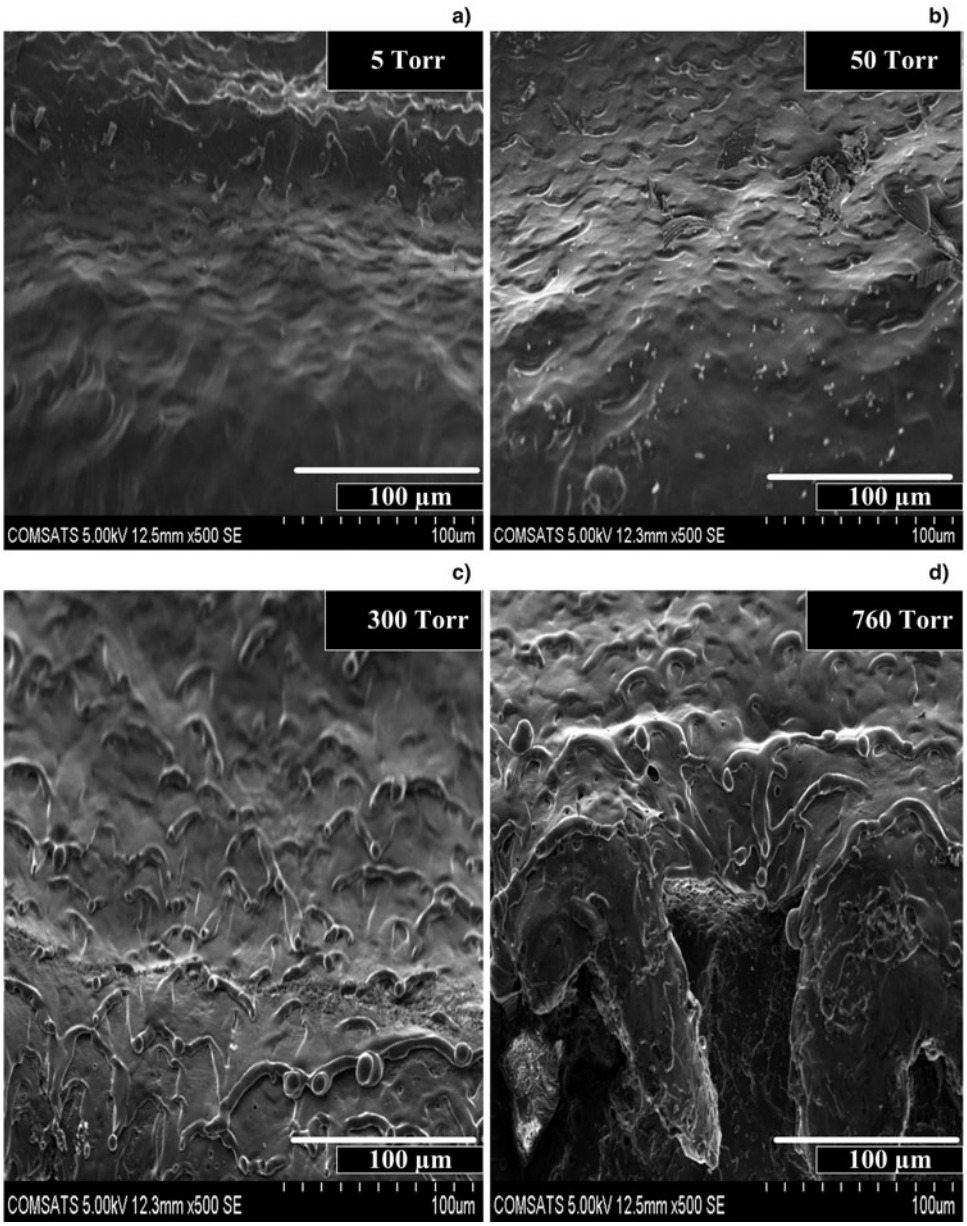

Fig. 2. SEM image revealing surface morphology of the centrally ablated area of Mg-alloy under Ar ambient, at a fluence of 1.3 J cm^{-2} for different pressures (a) 5, (b) 50, (c) 300, and (d) 760 Torr.

pressure micro-sized cavities, islands with non-uniform shape and density distribution are observed as shown in Figure 5a. When the pressure increases, the size of cavities increases and their density decreases. These cavities become less distinct and merged as shown in Figures 5c and 5d and on the other hand islands have wiped out as revealed in Figures 5c and 5d. Figure 5c depicts the formation of micro-sized droplets formation at 300 Torr and they are vanished at the highest pressure of 760 Torr (Fig. 5d). Non-uniform redeposition of ablated material.

SEM micrographs of Figures 6a–6d display centrally ablated area of Mg-alloy under He after irradiation at a fluence of 1.3 J cm^{-2} for different pressures of (a) 5, (b) 50, (c) 300, and (d) 760 Torr. For the pressure 5 & 50 Torr micro-sized and unorganized ripples and droplets are observed in Figures 6a and 6b. Figures 6c and 6d exhibit the formation of ridges at 300 and 760 Torr. Redeposition of ejected material is also observed at these pressures. However, droplet formation is vanished for highest pressures.

The SEM micrographs of Figures 7a–7d represent peripheral ablated area of Mg-alloy under He environment after irradiation at a fluence of 1.3 J cm^{-2} for different pressures of (a) 5, (b) 50, (c) 300, and (d) 760 Torr, respectively. For the lowest value of pressure 5 Torr, micro-sized cones, cavities, and island with non-uniform shape and density distribution are observed as shown in Figure 7a. As shown in Figures 7b and 7c, when the pressure increases the density of cavities increases, whereas appearance of both cones and cavities

https://doi.org/10.1017/S0263034615000312 Published online by Cambridge University Press

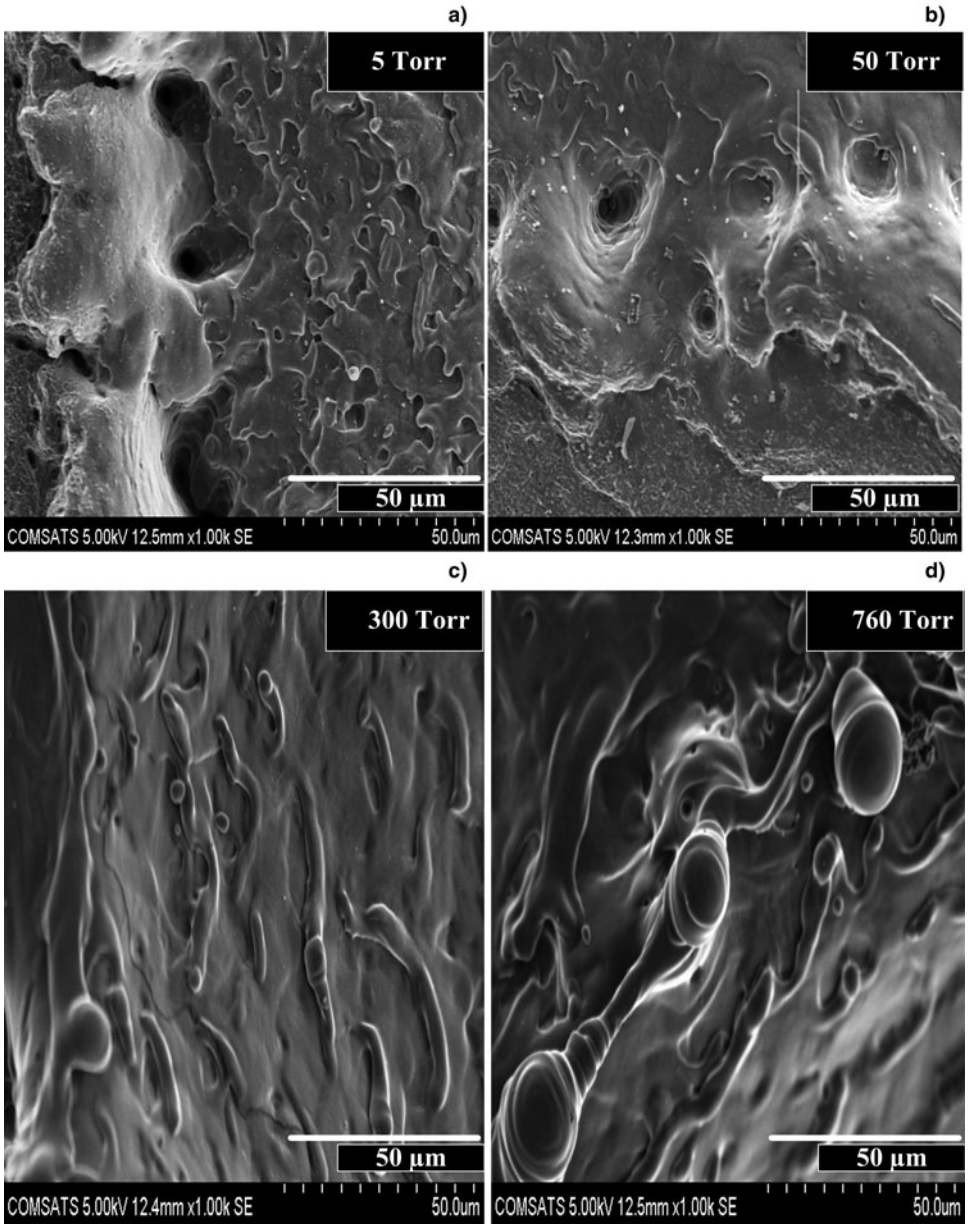

Fig. 3. SEM image revealing surface morphology of the peripheral ablated area of Mg-alloy under Ar environment, at a fluence of 1.3 J cm^{-2} for different pressure of (a) 5, (b) 50, (c) 300, and (d) 760 Torr.

become more distinct and well defined as compared with Figure 7a. Figure 7c depicts that for high-pressures of 300 Torr these islands again become less prominent, whereas the cavities with non-uniform shape and density distribution are with distinct appearance as seen. Figure 7d also depicts that for highest pressure 760 Torr islands and cones are completely vanished and only droplets are seen.

Ripple formation as shown in Figures 2, 4, and 6a–6d can be explained on the basis of interaction between incoming laser radiation and laser-induced surface plasmons (Akram *et al*., 2014). A critical density of electrons may present near specimen surface during laser interaction. At normal incidence the laser electric field would excite oscillations parallel to the surface. Surface irregularity might cause laser light to be dispersed tangentially to the surface, which could yield a standing wave pattern. The merged incident, reflected and diffracted waves could combine to give an electric field distribution able to generate localized plasma oscillations. This consequences into the formation of ripples on the ablated surface (Kalsoom *et al*., 2012).

Hydro-dynamical instabilities (Kelvin–Helmholtz instability) are also responsible for the growth of such kind of structures (ripples) (Liu *et al*., 2011). Ridges formation as shown in Figure 6 is due to enhanced recoil pressure of the plasma which causes more material splashing toward the boundary (Yu & Lu, 1999). An increase in the density of

https://doi.org/10.1017/S0263034615000312 Published online by Cambridge University Press

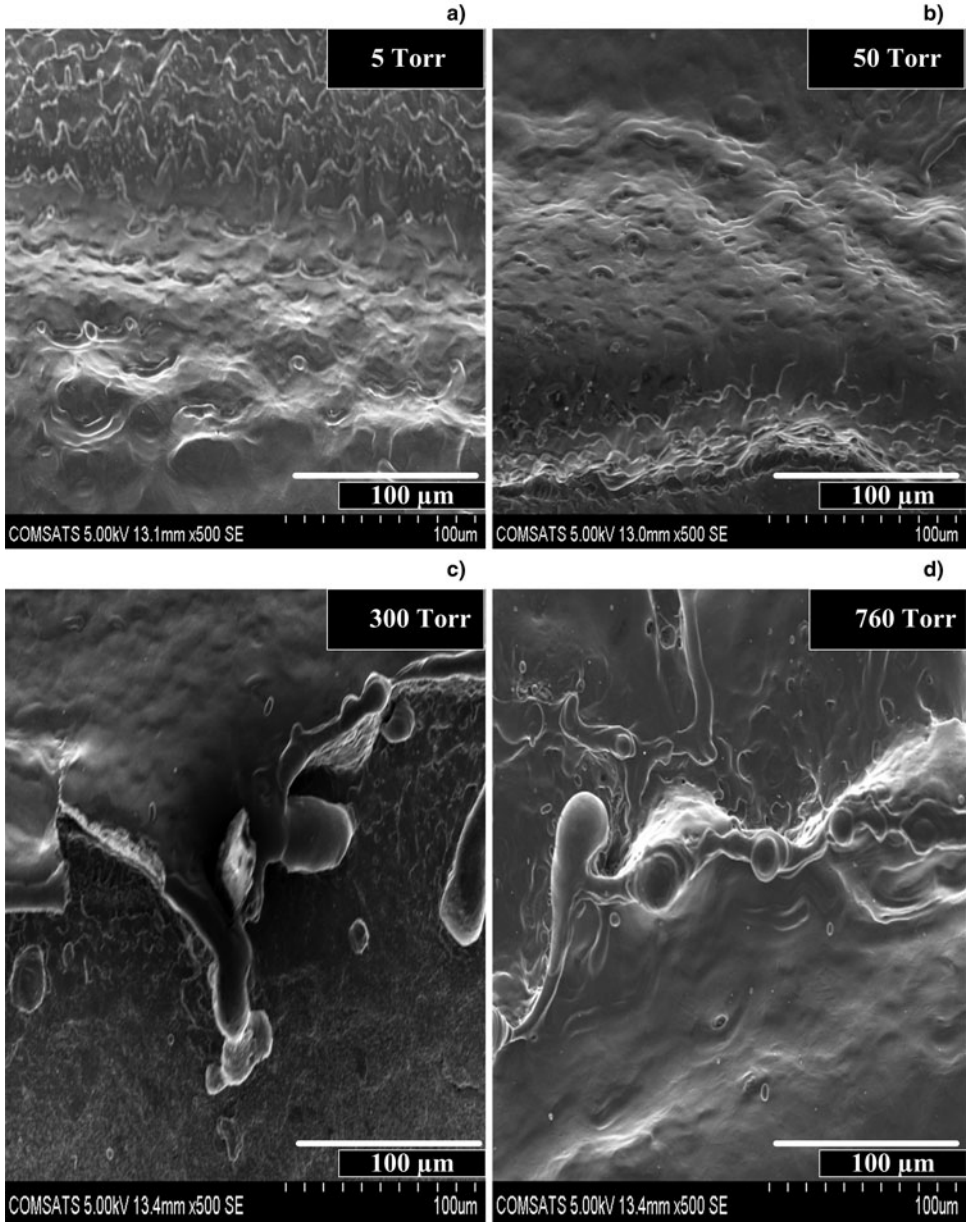

Fig. 4. SEM image revealing variation of surface morphology of the centrally ablated area of Mg-alloy under Ne environment, at a fluence of 1.3 J cm^{-2} for different pressures (a) 5, (b) 50, (c) 300, and (d) 760 Torr.

these ripples and ridges is attributed to enhanced energy deposition (Yu & Lu, 1999). The density of ripples and ridges that reduces at higher pressures is due to large-scale melting, re-solidification, and correspondingly merging of individual periodic structures with each other as shown in Figures 2, 4, and 6 (Huang *et al*., 2010).

Formation of cavities is attributed to thermal ablation on the basis of laser-induced heating, melting, explosive boiling, and thermal desorption of the target surface (Chrisey & Hubler, 1994). Cavity formation can be explained on the fact that as the plasma/vapor pressure exceeds from the surrounding pressure; the molten material can be expelled explosively from the target due to the violent recoil pressure (Körner *et al*., 1996). The variation in the size of cavities is ascribed to the large number of surface defects, such as contaminants, inclusions, and small pits (Dauscher *et al*., 1996). The increasing pressure, and increase in density is attributed to increase in recoil pressure, whereas decrease is attributed to redeposition of ablated material. These cavities vanish at the highest value of pressure due to refilling of the melted material (Yousaf *et al*., 2013). Hydro-dynamic sputtering, defects and ablation due to evaporation resistive impurities are attributed to cones formation (Dolgaev *et al*., 2006). The density of observed cones increases with the increase in ambient gas pressure which is due to enhanced energy deposition.

Islands formation with non-uniform shapes and sizes on the laser-irradiated surface of the material is due to

https://doi.org/10.1017/S0263034615000312 Published online by Cambridge University Press

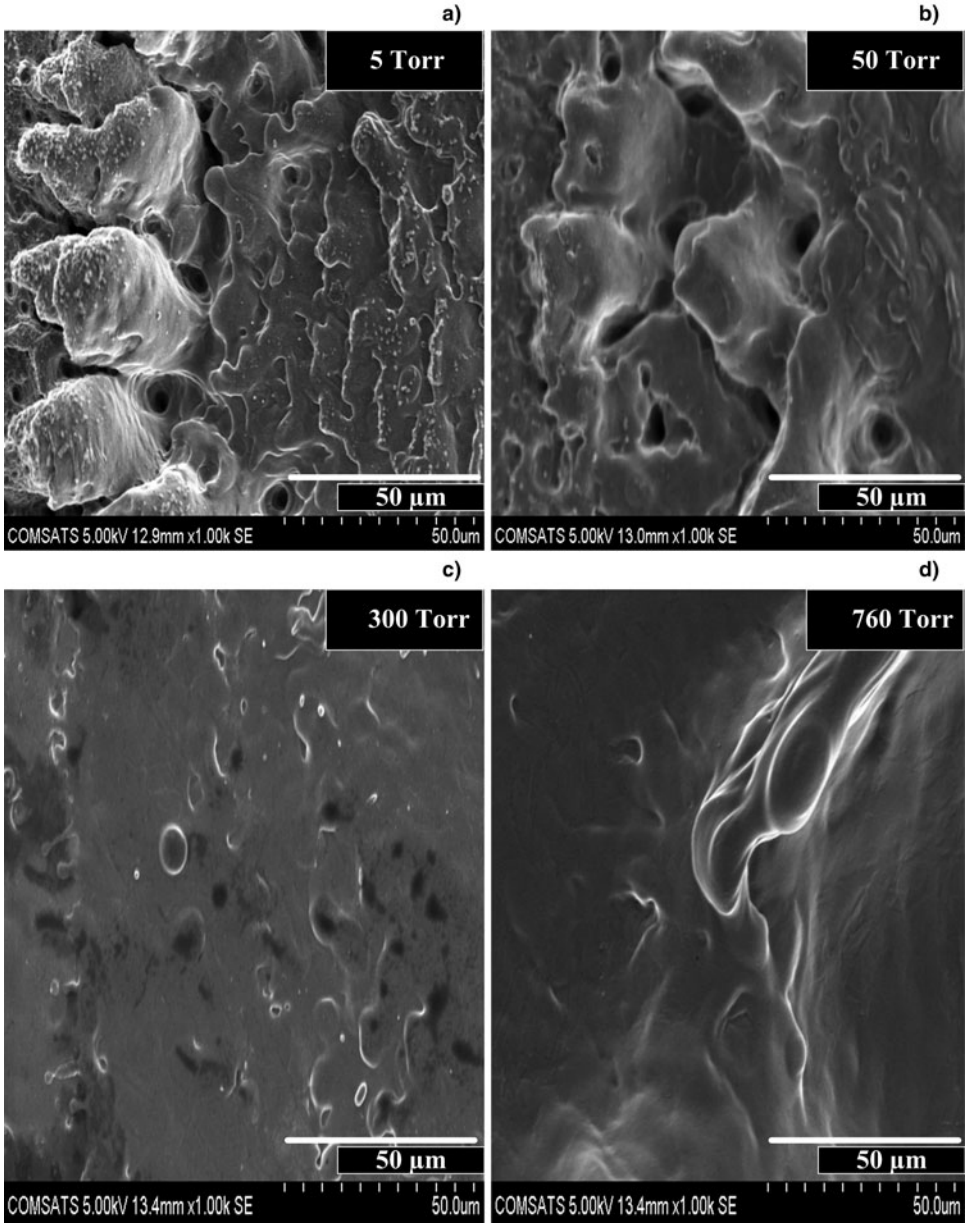

Fig. 5. SEM image revealing surface morphology of the peripheral ablated area of Mg-alloy under Ne environment, at a fluence of 1.3 J cm^{-2} for different pressure of (a) 5, (b) 50, (c) 300, and (d) 760 Torr.

exfoliational sputtering (Shaheen *et al.*, 2013). The aggregation of such large-sized droplets is due to large-scale melting and resolidification on surface structures.

The formation of droplets is attributed to a transition from a vaporization-dominated ablation regime to a regime where melt-expulsion concurs, and "hydro-dynamical" sputtering becomes dominant. This hydro-dynamical mechanism refers to the formation and liberation of micro-size droplets from the melt at the surface of material (Bleiner & Bogaerts, 2006).

From Figures 2 to 7 various kind of structures such as ripples, ridges, cavities, cones, islands, and droplets are observed in different environments of Ar, Ne, and He. These structures are most distinct in case of Ar, then Ne followed by He. The difference in surface modification of Mg-alloy is due to ionization potential (E), thermal conductivity (k), and E/M ratio of environmental gases (Ar, Ne, and He) where E is energy of the first ionization state, M is the mass of gas.

The ablation of Mg-alloy in case of Ar is responsible for the growth of more distinct feature due to more energy deposition of Ar-plasma to the lattice of Mg-alloy as compared with Ne- and He-plasma. The more energy deposition is correlated with favorable cascade growth and consequently more excitation temperature as well as number density of plasma species. In case of Ar, the cascade is more favorable due to smaller values of (E/M ratio = 0.53, E = 15.546 eV) from Eq. (7) as compared with Ne and He.

https://doi.org/10.1017/S0263034615000312 Published online by Cambridge University Press

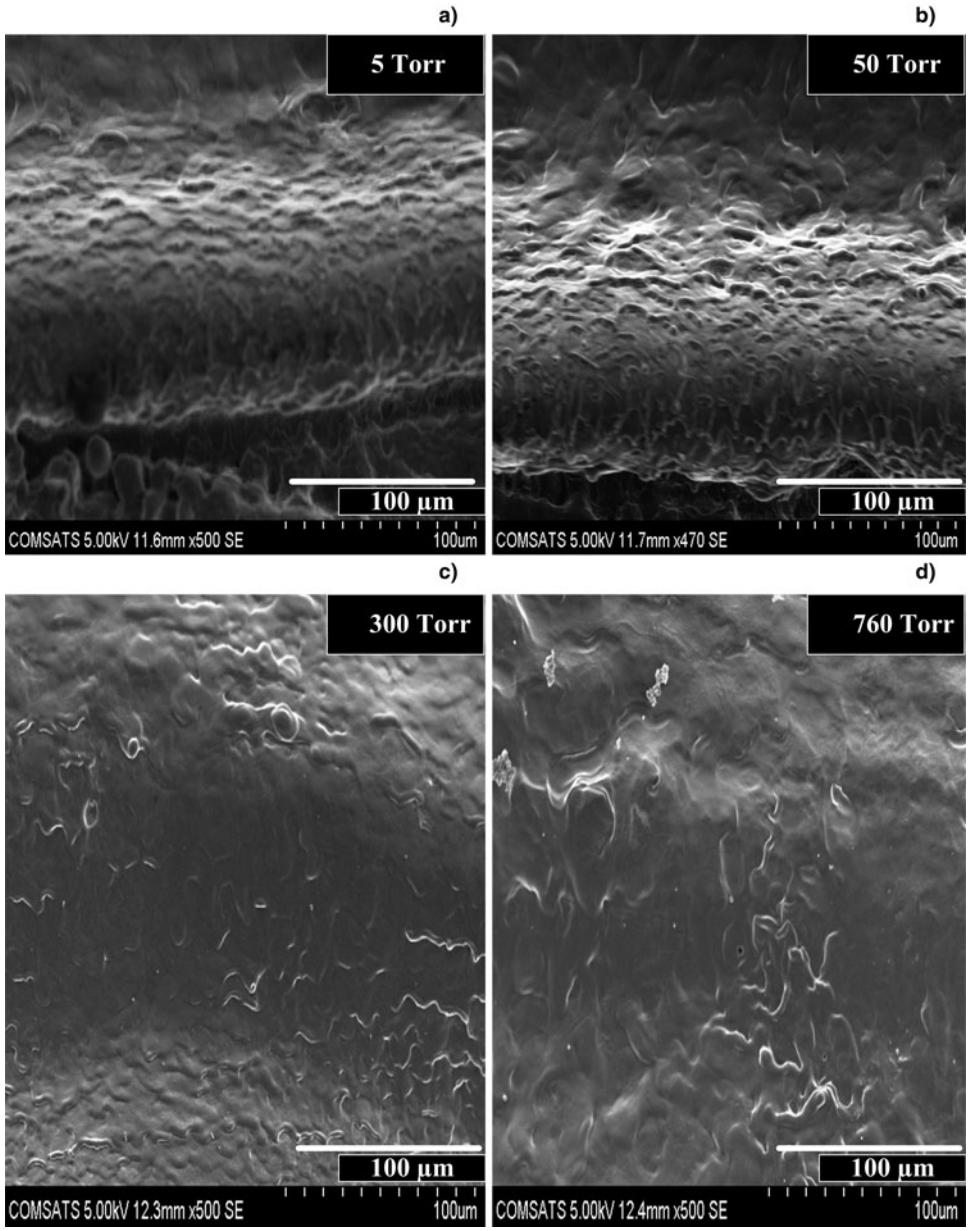

Fig. 6. SEM image revealing variation of surface morphology of the centrally ablated area of Mg-alloy plasma under He ambient, at a fluence of 1.3 J cm^{-2} for different pressures (a) 5, (b) 50, (c) 300, and (d) 760 Torr.

Similarly the other factor which is responsible for the different growth structures is the thermal conductivity of environmental gases. The higher thermal conductivities of He [151.3(W $m.K^{-1}$)] as compared with Ne [49.1(W $m.K^{-1}$)] and Ar [17.72(W $m.K^{-1}$)] will be more heat dissipation losses and fast cooling of plasma. Therefore, the *K.E* loss will be more significant in case of He as compared with Ne and Ar (Farid *et al.*, 2012).

3.2. Effects of Nature and Pressure of Ambient Environments on Plasma Parameters

The ambient environments and pressure are the controlling parameters of emission intensity, electron temperature, and electron number density (Shaikh *et al.*, 2006). In our experiment, all parameters laser fluence of 1.3 J cm^{-2} was kept constant. Initially we performed our experiments in all environments of Ar, Ne, and He and found that at a fluence of 1.3 J.cm^{-2} the emission intensity of Mg-alloy plasma is maximum. By increasing fluence from 1.3 J cm^{-2}, it is observed that emission intensity of Mg-alloy plasma decreases. Therefore this fluence was considered as optimum fluence and hence all the measurements related to variation in pressures were performed under this optimum fluence. With increasing laser irradiance more excited species, ions, and free electrons are generated that interact with incoming laser photon, leading to further heating and ionization and resulting in an increase in the absorption of

https://doi.org/10.1017/S0263034615000312 Published online by Cambridge University Press

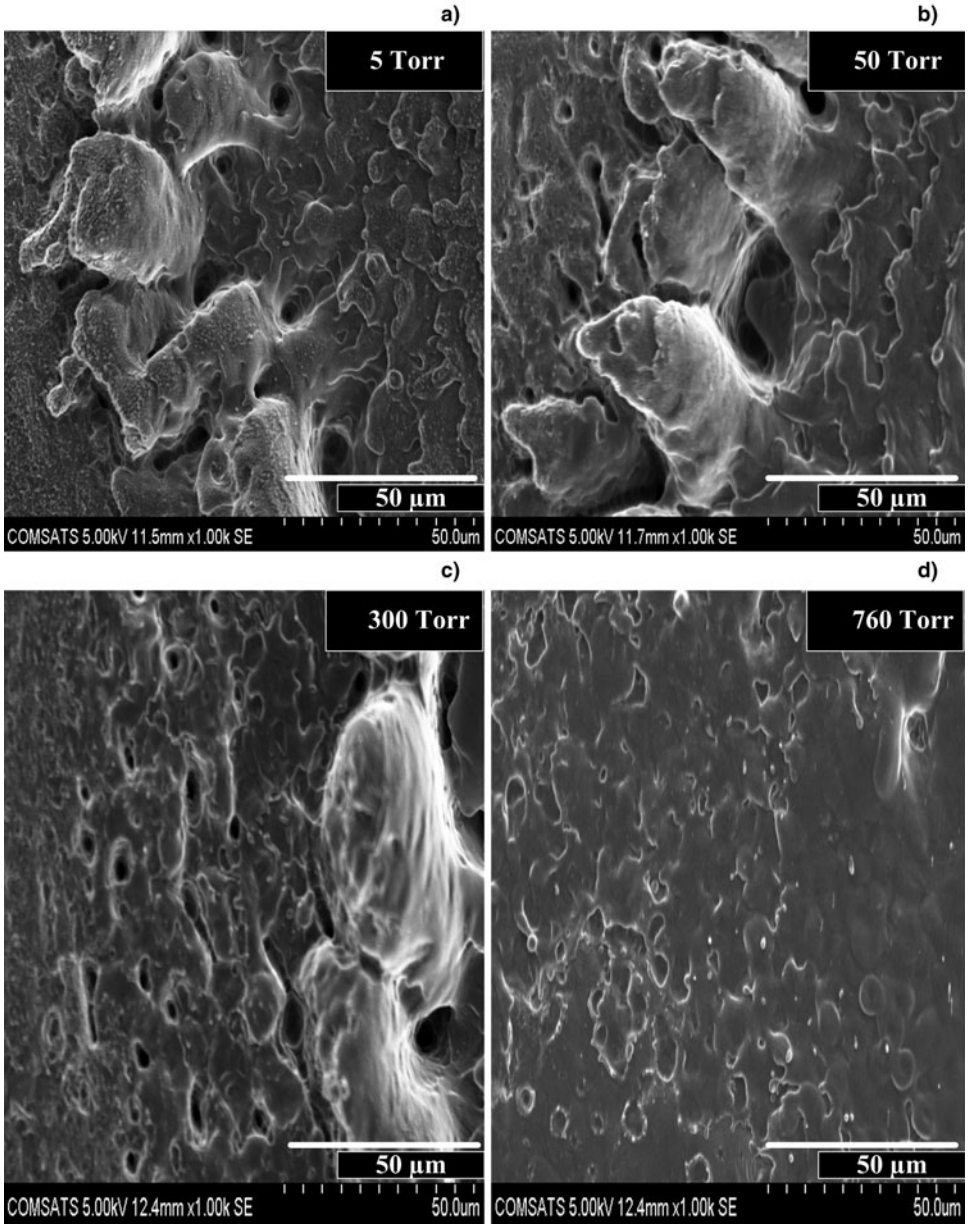

Fig. 7. SEM image revealing surface morphology of the peripheral ablated area of Mg-alloy under He environment, at a fluence of 1.3 J cm^{-2} for different pressure of (a) 5, (b) 50, (c) 300, and (d) 760 Torr.

the laser energy. The plasma progressively behaves like an optically thick medium and effectively shields the target surface from the tailing part of laser pulse (Hafeez *et al*., 2008).

Similarly, LIBS analysis of Mg-alloy was performed by varying delay times under all environment of Ar, Ne, and He. At a time delay of 2.01 µs the maximum emission intensity and correspondingly electron temperature and electron number density were observed. Therefore this delay time was considered as most favorable delay time and therefore all measurements related to pressure variation are performed under this delay time. Due to transient nature of laser-induced plasma its evolution can be subdivided into three steps: Breakdown, expansion, and confinement. During ablation when target breakdown is obtained and material is ejected, the laser pulse is still on, heating the free electrons to temperatures of the order of a few tens of thousands kelvin depending on the laser photon energy. In this stage, the ionization degree is close to unity as a consequence of the kinetic mechanisms involved in the breakdown process and of the extremely high number density of ejected atomic gas. When the laser pulse has ended, the degree of ionization is found to be much higher than the corresponding equilibrium value at the observed electron temperature. During the phase of plasma expansion, despite the cooling due to collisions with cold ambient gas atoms, the variation of particle

https://doi.org/10.1017/S0263034615000312 Published online by Cambridge University Press

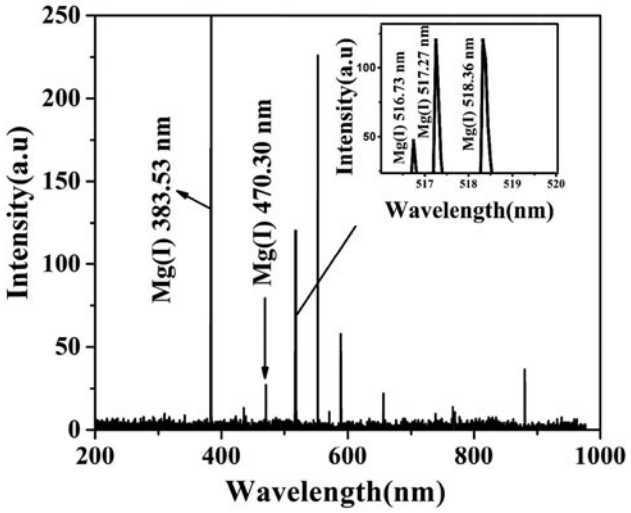

Fig. 8. The optical emission intensity spectrum of the laser-irradiated Mg-alloy plasma in an ambient environment of He at a pressure of 5 Torr at a fluence of 1.3 J.cm^{-2}.

number density and gas temperature is predominantly produced by the physical expansion of the high-pressure ablated material in the surrounding environment. As a matter of fact during the initial expansion stage, all the processes with an associated time longer than microsecond could not reach equilibrium as a consequence of the fast change of plasma particle number density and temperature. After the first stage of expansion, the plasma front stops while the shock wave continues moving in the ambient gas. At this stage the volume occupied by the plume keep the same approximate dimension for several microseconds. In this period, the variation rate of the thermodynamic parameters is mainly due to the plasma cooling effect, resulting from collisions with cold atoms in the ambient gas. This rate is markedly lower than that in the expansion phase (Cristoforetti *et al*., 2010).

The distance of probe from target is kept constant. The only changing parameters are ambient environments (Ar, Ne, He) and the corresponding pressure ranging from 5 to 760 Torr.

Figure 8 reveals the emission spectra of laser-irradiated Mg-alloy plasma obtained at pressure of 5 Torr under ambient environment of He at a fluence of 1.3 J.cm^{-2}. Five spectral lines from neutral Mg atoms are selected that is, 383.53, 470.30, 516.73, 517.27, and 518.36 nm and are labeled in the main spectrum as well as in the inset of Figure 8 (Reader *et al*., 1980).

3.2.1. *Investigation of Emission Intensity*

Figure 9 shows the effect of ambient environments and pressure on the emission intensity of Mg-alloy plasma. These emission intensity spectra are taken under ambient environments of (a) Ar, (b) Ne, and (c) He at a constant fluence of 1.3 J.cm^{-2}, respectively. Mg lines with wavelength of 383.53, 470.30, 516.73, 517.27, and 518.36 nm, respectively, are used. It is observed that emission intensity initially increases with the increasing pressure; attains its maxima at 20 Torr and then decreases. Finally it achieves saturation with further increase in pressure up to 760 Torr. Maximum emission intensity is achieved for spectral line of 383.53 nm. For other lines a very slight increase and then saturation is observed. It is also clear that emission intensity of all spectral lines in case of Ar is significantly higher than Ne and He.

3.2.2. *Investigation of Electron Temperature*

The excitation temperature has been evaluated by employing the Boltzmann plot method on spectroscopic data (Harilal *et al*., 1998*a*; 1998*b*) by assuming the validity of the condition of the local thermodynamic equilibrium (LTE) and calculation has been carried out using a following relation (Harilal *et al*., 1998*a*; 1998*b*).

$$\ln\left(\frac{\lambda_{mn} I_{mn}}{g_m A_{mn}}\right) = -\left(\frac{E_m}{kT_e}\right) + \ln\left(\frac{N(T)}{U(T)}\right), \quad (1)$$

where on the left-hand side λ_{mn}, I_{mn}, g_m, and A_{mn} are the wavelength, intensity of the upper energy state m, statistical weight, and transition probability, respectively. On the right-hand side E_m, k, T_e, N (T), and U (T) are energy of upper state, Boltzmann constant, electron temperature, total number density, and partition function, respectively.

The related spectroscopic parameters for the transitions of the laser-induced Mg-alloy plasma used in calculations have been taken from the NIST database (Reader *et al*., 1980; Kaufman & Martin, 1990) and are listed in Table 2.

Figure 10 depicts the variation in the evaluated electron temperatures of Mg-alloy plasma for various pressures ranging from 5 to 760 Torr under three ambient environments of Ar, Ne, and He at a fixed fluence of 1.3 J cm^{-2}, respectively.

The emission lines chosen for the calculation of electron temperature fulfill criterion (Lacroix *et al*., 1997; Sabbaghzadeh *et al*., 2007)

$$E_1 - E_2 = kT_{exc}, \quad (2)$$

where E_1 is energy of the upper level of emission line 1., E_2 energy of the upper level of emission line 2, $\boldsymbol{k}$ the Boltzmann constant, and T_{exc} the excited temperature.

By choosing two emission lines at wavelength of 470.30 and 516.73 nm the value of $E_1 - E_2$ comes out to be 1.87352 eV and value of kT_{exc} is 1.10775 eV which fulfills criteria of Eq. (2).

In the case of Ar, the electron temperature varies from 8167 to 12,855 K. With increasing pressure a slight increase in electron temperature is observed and achieves its maxima at 10 Torr. Afterwards it decreases till 50 Torr and then the saturation is achieved up to 760 Torr. In the case of Ne, the

https://doi.org/10.1017/S0263034615000312 Published online by Cambridge University Press

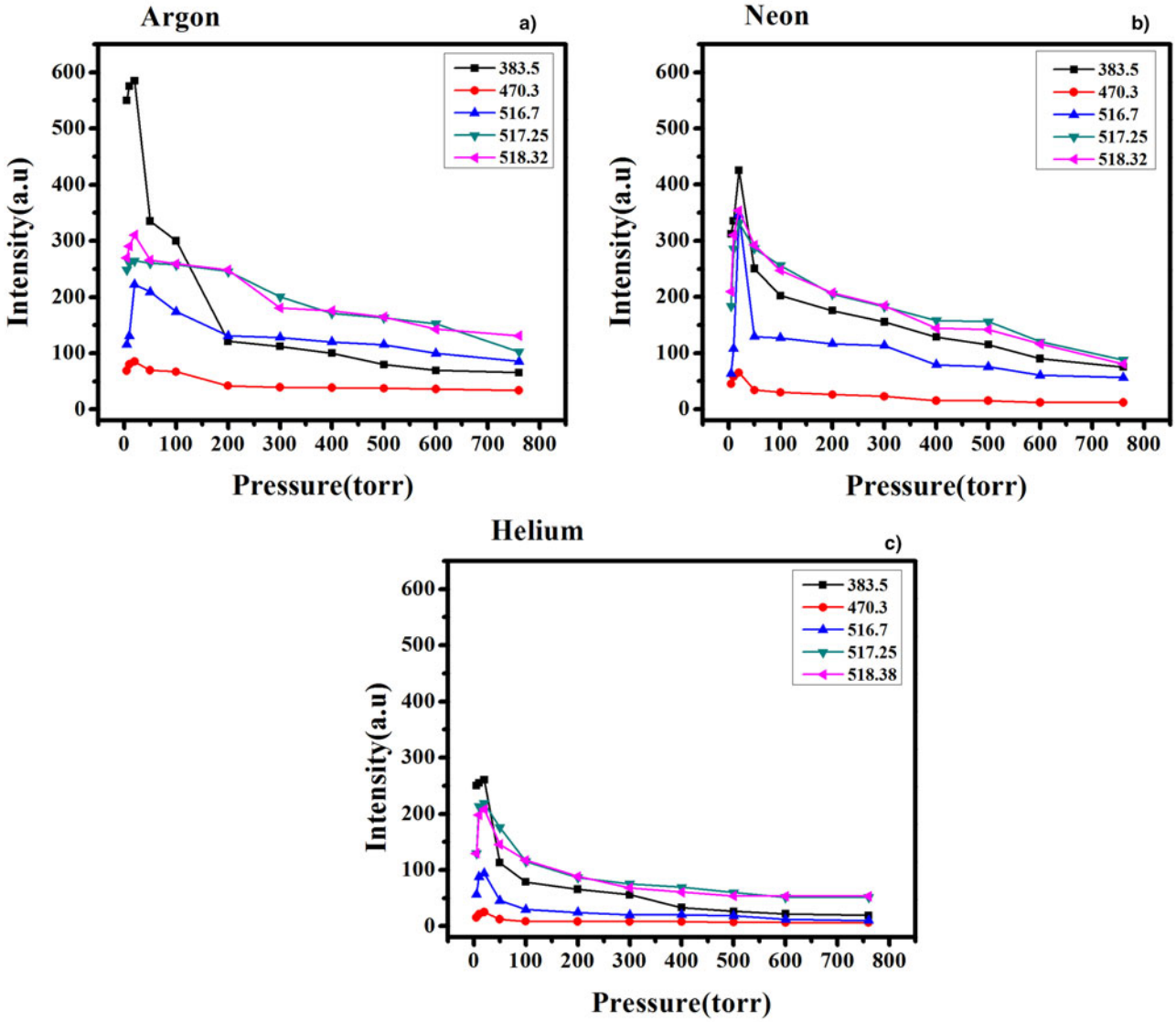

Fig. 9. The variation in emission spectral intensities of the laser-irradiated Mg-alloy plasma for various pressures under ambient environment of (a) Ar, (b) Ne, and (c) He at a fluence of 1.3 J cm^{-2}.

electron temperature varies from 6725 to 10,834 K. With the increasing pressure of Ne electron temperature increases and achieves its maxima at 10 Torr. Afterwards it decreases and finally attains saturation. For He the electron temperature varies from 6628 to 10,718 K. The trend is almost similar to Ar and Ne.

The highest value of electron temperature is observed for Ar, for Ne, and then for He for all pressures.

Table 2. *The spectroscopic data of laser-induced Mg-alloy plasma taken from NIST database (Kaufman & Martin, 1990; Reader et al., 1980)*

Wavelength (nm)	Transitions	Terms	Energy of upper level, E_m (cm^{-1})	Statistical weight, g_m	Transition probabilities (10^8 S^{-1})
383.53	$3s3p-3s3d$	$^3p^o$–^{3}D	47,957	15	1.68
470.30	$3s3p-3s5d$	$^1p^o$–^{1}D	56,308	5	0.255
516.73	$3s3p-3s4s$	$^3p^o$–^{3}S	41,197	3	0.116
517.27	$3s3p-3s4s$	$^3p^o$–^{3}S	41,197	3	0.346
518.36	$3s3p-3s4s$	$^3p^o$–^{3}S	41,197	3	0.575

https://doi.org/10.1017/S0263034615000312 Published online by Cambridge University Press

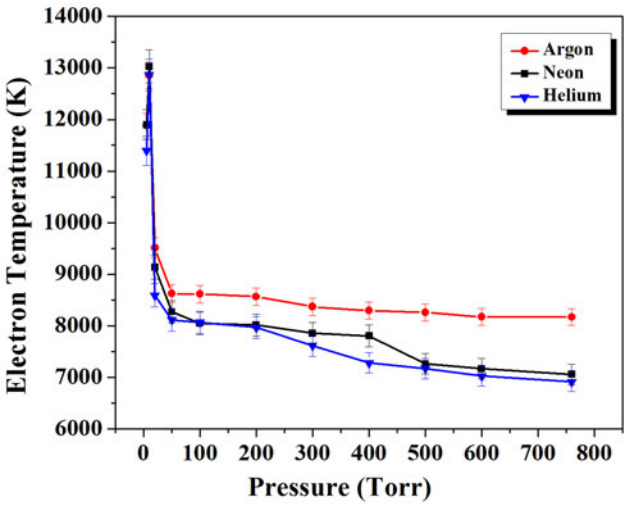

Fig. 10. The variation in electron temperature of the laser-induced plasma of Mg-alloy for different pressures ranging from 5 Torr to 760 Torr under three ambient environments of Ar, Ne, and He at a fluence of 1.3 J cm^{-2}.

3.2.3. *Investigation of Electron Number density*

The electron number density of the Mg-alloy plasma due to the Stark broadening mechanism of emission spectra can be evaluated by following relations for full width half maximum (FWHM) (Nakimana *et al.*, 2012).

$$\Delta\lambda_{1/2} = 2\omega\left(\frac{N_e}{10^{16}}\right) + 3.5A\left(\frac{N_e}{10^{16}}\right)^{1/4}\left[1 - 1.2N_D^{-1/3}\right] \times \omega\left(\frac{N_e}{10^{16}}\right), \quad (3)$$

where $\Delta\lambda_{1/2}$ is the FWHM, N_e is the electron number density (cm^{-3}) ω is the electron impact width parameter, and A is the ion broadening parameter. Where N_D is the number of particles in the Debye sphere and can be calculated by the following relation (Shaikh *et al.*, 2007):

$$N_D = 1.72 \times 10^9 \frac{T_e^{(3/2)}(\text{eV})}{N_e^{(1/2)}(\text{cm}^{-3})} \quad (4)$$

The first term in Eq. (3) is related with electron broadening and second with ion broadening but in our case ion broadening is negligible (Griem, 1997), so Eq. (3) reduces to,

$$\Delta\lambda_{(1/2)} = 2\omega\left(\frac{N_e}{10^{16}}\right). \quad (5)$$

The Mg(I) line of 517.27 nm wavelength is used for the calculation of electron number density after insuring that particular line is not broadened and having well-fitted shape according to Lorentzian function, which indicates that self-absorption phenomenon is negligible.

The condition that the atomic and ionic sates should be populated and depopulated predominantly by the electron collisions, rather than by radiation, requires an electron number density that is sufficient to ensure the high collision rate.

The necessary condition for fulfilling the condition of LTE is McWhirter criteria (Huddlestone & Leonard, 1965).

$$N_e \geq 1.6 \times 10^{12}\, T_e^{(1/2)} \Delta E^3 \ \text{cm}^{-3}, \quad (6)$$

where T_e is the plasma temperature in K and ΔE (eV) is the energy difference between the excited and ground states that are likely to be in LTE. At Te = 12 855 K (the highest calculated temperature), the electron number density comes out to be $N_e \sim 2.503 \times 10^{15}$ which describes the legitimacy of LTE.

Figure 11 exhibits the resulting calculated electron number density of Mg-alloy plasma at different pressures under three ambient environments of Ar, Ne, and He at a fluence of 1.3 J cm^{-2}. Values of electron number density range from 7.74×10^{17} to 19.17×10^{17} cm^{-3} for Ar, from 7.58×10^{17} to 10.07×10^{17} cm^{-3} for Ne, and from 5.40×10^{17} to 10.45×10^{17} cm^{-3} for He. In case of Ar by increasing pressure the electron number density increases, achieves its maxima at 760 Torr. In the case of Ne, number density increases slightly and attains its maxima at 200 Torr. Then it decreases slightly and saturation behavior is observed up till 760 Torr. Whereas in case of He the number density increases with increasing pressure and maxima is achieved at 50 Torr. With further increase in pressure a decrease in number density is observed. Afterwards again it shows a saturation behavior up till 760 Torr.

The results attained from LIBS show that emission spectra, electron temperature, and electron number density are

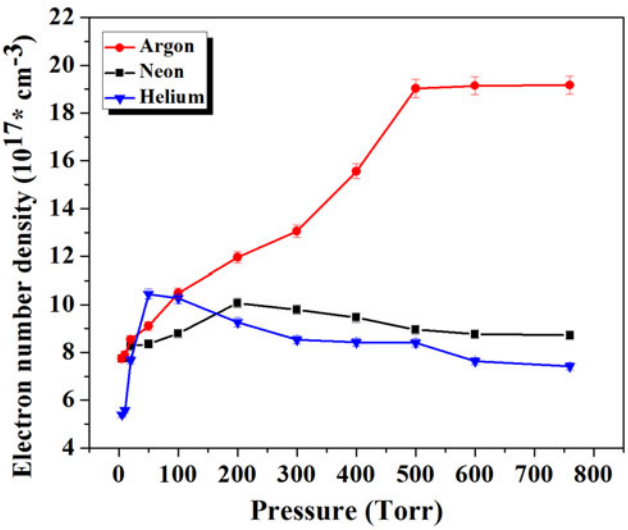

Fig. 11. The variation in the electron number density of laser-induced plasma of Mg-alloy at different pressures under three ambient environments of Ar, Ne, and He, at a fluence of 1.3 J cm^{-2}.

https://doi.org/10.1017/S0263034615000312 Published online by Cambridge University Press

strongly dependent on the nature and pressure of ambient environments. The highest values of plasma parameters for example, emission intensity, electron temperature, and electron number density are associated with Ar, then with Ne, and the least value is obtained for He.

The trend of emission intensity and electron temperature can be divided into three different regimes; in the first regime they increase with the increasing pressure of ambient environment. In the second regime, it decreases with increase in pressure. In the third regime, the saturation is achieved without any significant change. The emission intensities are effected by the amount of vaporized material which is controlled by extent of shielding effect of the ambient plasma, temperature changes due to absorption of laser radiation into the plasma and changes in plasma expansion mode (laser supported combustion wave, laser supported detonation wave, and laser supported radiation wave) (Iida, 1990). The initial increase in emission intensity with the increase of pressure is observed and its maxima is achieved at 20 Torr which is attributed to the enhanced collisional excitation/dexcitation and confinement of the plume species at these pressures. Afterwards, further increase in pressure up to atmospheric pressure (760 Torr) leads to reduction in the line intensities. The more pronounced confinement effect now leads to the shielding effect which reduces the fraction of laser energy available to reach the target surface and hence reducing the amount of material being vaporized. A greater amount of energy is screened by the plasma and less energy is absorbed by the target at higher pressure and is responsible for reduction in emission line intensities. In addition to this, the decrease in the intensity at higher pressures can also be correlated with the decrease in temperature observed at higher pressures due to increased recombination losses. The decrease in emission intensity after 20 Torr is correlated with the self-absorption phenomenon which becomes dominant at higher pressures (Hafeez *et al*., 2008; Farid *et al*., 2014; Harilal *et al*., 2014). The same trend is observed for electron number density except in case of Ar, in which it goes on increasing with increasing pressure. It is observed that plasma attains its maximum temperature at 10 Torr for all ambient environments.

The obtained results from the LIBS indicate that the emission intensity, electron temperature, and density are strongly dependent on ambient atmosphere as well as on its pressure variation. The highest value of the emission intensity, excitation temperature, and electron number density has been observed for Ar, then for Ne, and the least for He.

The initial increase in emission intensity, excitation temperature, and electron number density is attributable to the restricted free expansion and confinement effects of plasma (Harilal *et al*., 1998*a*; 1998*b*). With increasing pressure, collisional frequencies of plasma species are also enhanced which are responsible for enhanced momentum transfer and cascade growth (Weyl, 1989). When the maxima is achieved a decrease in plasma parameters is observed. This decreasing trend is attributable to more pronounced confinement effect of the plasma species nearer to the target as a result the shielding effect near target surface takes place. Thus less amount of laser energy is being absorbed in the target material and reduces the values of excitation temperature and electron number density (Cowpe *et al*., 2009). With further increase in pressure up to 760 Torr, the saturation or insignificant change in plasma parameters is observed which is due to the self-regulating regime along with plasma shielding effect (Harilal *et al*., 1998a, 1998*b*). In addition, breakdown of the ambient gases serves as a buffer and transfers more amount of energy to the target surface by thermal ionization which leads toward increase in emission intensity, excitation temperature, and electron number density(Harilal *et al*., 1997).

The nature of environment also influences plasma parameters significantly. This trend is also explainable on the basis of cascade growth and necessary condition for cascade growth is given by the following formula (Iida, 1990; Farid *et al*., 2012):

$$\frac{d\varepsilon}{dt} = \frac{4\pi^2 e^2 I \nu_{\text{eff}}}{m_e c \omega^2} - \frac{2 m_e \nu_{\text{eff}} E}{M} \tag{7}$$

where ε is the energy of the free electrons, m and e are the mass and charge of the electron, M is the mass of the background gas neutral particle, and E is the energy of the first ionization stage of gas, I is the radiation intensity, ω the cyclic frequency of radiation and υ_{eff} the effective frequency of electron–neutral collisions. The first term on the right-hand side of Eq. (7) represents the rate of growth of energy by the absorption of the laser pulse. This term remains constant for all ambient environments. So the second part is important and in this part E/M is influential factor to calculate amount of energy loss in cascade growth process. In the case of Ar it is 0.53, for Ne it is 1.08, and for He it is 6.04. This shows that cascade growth is more favorable for Ar, then for Ne, and He (Bashir *et al*., 2012; Iida, 1990). It explains the fact that the Mg-alloy plasma has more emission intensity, $K.E$ as well as density in case of Ar as compared with Ne and He.

Another controlling factor of loss of energy is thermal conductivity. The thermal conductivity scales as He [151.3 W $(\text{m.K})^{-1}$] > Ne [49.1 W $(\text{m.K})^{-1}$] > Ar [17.72 W $(\text{m.K})^{-1}$]. As higher will be the conductivity lower will be the cascade growth and higher will be the heat dissipation losses near the surface and as a consequence lower will be kinetic energies of plasma for He, then for Ne, and higher will be for Ar (Bashir *et al*., 2012).

LIBS analysis is well correlated with the surface modification of Mg-alloy after laser irradiation. The highest value of electron temperature and electron number density is achieved in Ar, then in Ne followed by He. In the case of Ar, this highest value of electron temperature and electron number density is justified by well-defined and distinct structures (Khan *et al*., 2013). The initial increase in electron temperature and electron number density with increasing pressure is

https://doi.org/10.1017/S0263034615000312 Published online by Cambridge University Press

well correlated with the formation of cavities, islands ripples (Khan *et al*., 2013). Higher electron temperature will be responsible for more deposition of energy to the lattice and large scale ablation will take place corresponding to increased depth and size of cavities. After obtaining the maxima, both electron temperature and electron number decrease and self-regulating regime is achieved. For this regime only redeposition of ablated material is obtained. Further increase in pressure, due to smaller value of electron temperature less energy deposition of electrons to lattice cause the growth of diffusive and less distinct structures (Khan *et al*., 2013).

3.3. Effect of Nature of Ambient Environment on Micro-Hardness

Figure 12 depicts the variation in micro-hardness of laser treated surface of Mg-alloy for different pressures under three ambient environments of Ar, Ne, and He at a fluence of 1.3 J cm^{-2}. The micro-hardness of un-irradiated specimen is 67 (HV). It is noticed that micro-hardness of laser-treated target is increased significantly as compared with the un-irradiated sample. It is observed that the micro-hardness also increases with increasing pressure, attains its maxima and then decrease with further increase in pressure in all ambient environments. The value of micro-hardness is achieved in case of Ar, that is, four times as compared with the irradiated target. The micro-hardness values in cases of Ne and He are two times than that of the un-irradiated sample. The changes in micro-hardness are attributed to the lattice disorder. These changes are also due to changes in crystal structure and thermal compressive stresses produced in the material as a result of laser-induced heating (Hull & Bacon, 2011). These micro-hardness results are well correlated with SEM as well as LIBS analysis. Distinct and well defined structures are observed in the case of Ar similarly the high value of electron temperature and electron number density is achieved in the case of Ar .The maximum value of plasma parameters is responsible for maximum surface and mechanical modification of laser-treated Mg-alloy in the case of Ar.

3.4. Effect of Ambient Gas on the Corrosion Resistance

Figure 13 illustrates the corrosion resistance of laser treated Mg-alloy under ambient environments of Ar, Ne, and He. The corrosion resistance of un-irradiated specimen is 0.03. However, it is observed that corrosion resistance is maximum in Ar, then in Ne followed by He as compared with un-irradiated sample. Improved corrosion resistance is attributed to phase change, microstructural refinement and extended solid solubility owing to rapid solidification (Mondal *et al*., 2008). These corrosion resistance results are well correlated with SEM morphology, LIBS analysis, and hardness.

4. CONCLUSIONS

The effect of nature and pressure of ambient environment that is, Ar, Ne, and He with pressure ranging from 5 to 760 Torr on surface structuring, plasma parameters, micro-hardness, and corrosion resistance of Mg-alloy targets is investigated. SEM investigation revealed the formation of craters, cavities, cones, droplets, and ripples at the central ablated region and island formation on the peripheral ablated area. At the low-pressure these structures were found to be more distinct due to enhanced energy deposition. These structures become diffusive with further increase in ambient gas pressure due to enhanced plasma shielding effect. Due to the

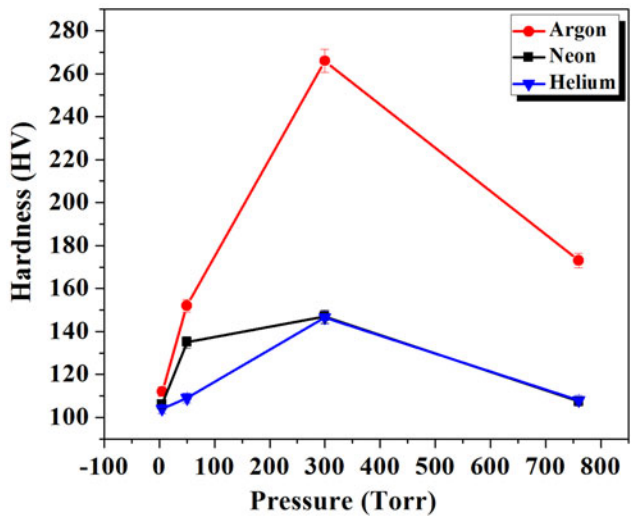

Fig. 12. The variation in micro-hardness of laser-irradiated Mg-alloy for different pressures under three ambient environments of Ar, Ne, and He, at a fluence of 1.3 J cm^{-2}.

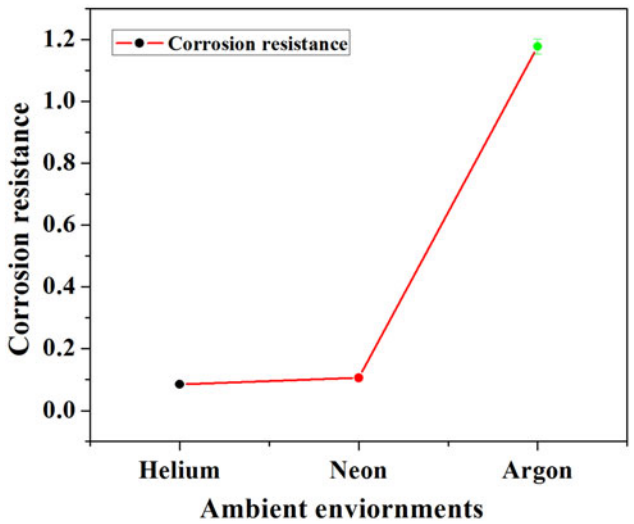

Fig. 13. The variation of corrosion-resistance of laser-induced plasma of Mg-alloy under three ambient environments of Ar, Ne, and He at a pressure of 5 Torr.

https://doi.org/10.1017/S0263034615000312 Published online by Cambridge University Press

Gaussian profile of laser beam, less energy deposition at periphery with increasing pressure causes enhanced ablation and the growth of large scale-structures. For LIBS analysis it is revealed that both electron temperature and electron number density increase with increasing pressure of ambient environment, attain their maxima, and then self-regulating region is achieved. The highest value of emission intensity, electron temperature, and electron number density of Mg-alloy plasma is obtained for Ar, then Ne, and He. SEM analysis is well correlated with LIBS analysis. The grown structures on Mg-alloy in Ar are more distinct, sharp, and well defined than in Ne and He. It can be attributed to more deposition of *K.E* of electrons to lattice due to enhanced electron temperature. In the same way, micro-hardness significantly increases after laser treatment. It is observed that the micro-hardness of Mg-alloy also increases with increasing pressure of gas, attains its maxima, and then decreases with further increase in pressure in all ambient environments. But in case of Ar environment micro-hardness of treated Mg-alloy is higher than in Ne and He. The corrosion resistance of the treated sample is increased than the untreated specimen. The highest value of corrosion resistance of Mg-alloy is attained in case of ablation in Ar where plasma parameters have maximum values and surface features are more distinct and well defined. Therefore it is concluded that nature and pressure of environmental gases play significant role for the growth of surface structures, generation and evolution of plasma, surface hardness, and corrosion resistance.

ACKNOWLEDGEMENT

We acknowledge Higher Education Commission of Pakistan for funding the project "Strengthening of Laser Facilities at GC University Lahore". We also acknowledge Director CASP and Sajjad Ahmad for providing the Hardness facilities

REFERENCES

Akram, M., Bashir, S., Hayat, A., Mahmood, K. & Ahmad, R. (2014). Effect of laser irradiance on the surface morphology and laser induced plasma parameters of zinc. *Laser Part. Beams*, **32**, 119–128.

Bashir, S., Farid, N., Mahmood, K. & Rafique, M.S. (2012). Influence of ambient gas and its pressure on the laser-induced breakdown spectroscopy and the surface morphology of laser-ablated Cd. *Appl. Phys. A*, **107**, 203–212.

Bleiner, D. & Bogaerts, A. (2006). Multiplicity and contiguity of ablation mechanisms in laser-assisted analytical micro-sampling. *Spectrochim. Acta B*, **61**, 421–432.

Chrisey, D.B., Hubler, G.K. (1994). *Pulsed Laser Deposition of Thin Films*. New York: John Willey & Sons.

Cowpe, J.S., Pilkington, R.D., Astin, J.S. & Hill, A.E. (2009). The effect of ambient pressure on laser-induced silicon plasma temperature, density and morphology. *J. Phys. D: Appl. Phys.*, **42**, 165202.

Cremers, D.A. (2014). *Space Applications of LIBS*. Heidelberg: Springer-Verlag.

Cristoforetti, G., Giacomo, A.D., Aglio, M.D., Lennaioli, S., Togoni, E., Palleschi, V. & Omenetto, N. (2010). Local thermodynamic equilibrium in laser-induced breakdown spectroscopy: Beyond the McWhirter criteria. *Spectrochim. Acta B*, **65**, 86–95.

Dauscher, A., Feregotto, V., Cordier, P. & Thomy, A. (1996). Laser induced periodic surface structures on iron. *Appl. Surf. Sci.*, **96–98**, 410–414.

Diwakar, P.K. (2014). *Laser Induced Breakdown Spectroscopy for Analysis of Aerosols*. Heidelberg: Springer-Verlag.

Dolgaev, S.I., Fernandez-Pradas, J.M., Morenza, J.L., Serra, P. & Shafeev, G.A. (2006). Growth of large micro cones in steel under multi pulsed Nd: YAG laser irradiation. *Appl. Phys. A*, **83**, 417–420.

Farid, N., Bashir, S. & Mahmood, K. (2012). Effect of ambient gas conditions on laser-induced copper plasma and surface morphology. *Phys. Scr.*, **85**, 015702–015709.

Farid, N., Harilal, S., Ding, H. & Hassanein, A. (2014). Emission features and expansion dynamics of nanosecond laser ablation plumes at different ambient pressures. *J. Appl. Phys.*, **115**, 033107.

Gondal, M.A. & Dastageer, M.A. (2014). *Elemental Analysis of Soils by Laser Induced Breakdown Spectroscopy*. Heidelberg: Springer-Verlag.

Griem, H.R. (1997). *Principles of Plasma Spectroscopy*. UK: Cambridge University Press.

Hafeez, S., Shaikh, N.M., Rashid, B. & Baig, M.A. (2008). Plasma properties of laser-ablated strontium target. *J. Appl. Phys.*, **103**, 083117–083124.

Harilal, S., Farid, N., Freeman, J., Diwakar, P., LaHaye, N. & Hassanein, A. (2014). Background gas collisional effects on expanding fs and ns laser ablation plumes. *Appl. Phys. A*, **117**, 319–326.

Harilal, S.S., Bindhu, C.V., Issac, R.C., Nampoori, V.P.N. & Vallabhan, C.P.G. (1997). Electron density and temperature measurements in a laser produced carbon plasma. *J. Appl. Phys.*, **82**, 2140–2146.

Harilal, S.S., Bindhu, C.V., Nampoori, V.P.N. & Vallabhan, C.P.G. (1998*a*). Temporal and Spatial behavior of electron density and temperature in a laser produced plasma from $YBa_2Cu_3O_7$. *Appl. Spectrosc.*, **52**, 449–455.

Harilal, S.S., Bindhu, C.V., Nampoori, V.P.N. & Vallabhan, C.P.G. (1998*b*). Influence of ambient gas on the temperature and density of laser produced carbon plasma. *Appl. Phys. Lett.*, **72**, 167–169.

Hark, R.R. & Harmon, R.S. (2014). *Geochemical Fingerprinting Using LIBS*. Heidelberg: Springer-Verlag.

Huang, M., Zhao, F., Cheng, Y., Xu, N. & Xu, Z. (2010). The morphological and optical characteristics of femtosecond laser-induced large-area micro/nanostructures on GaAs, Si and Brass. *Opt. Express*, **18**, A600–A619.

Huddlestone, R.H. & Leonard, S.L. (1965). *Plasma Diagnostic Techniques*. New York: Academic Press.

Hull, D. & Bacon, D.J. (2011). *Introduction to Dislocations*. UK: Oxford.

Iida, Y. (1990). Effects of atmosphere on laser vaporization and excitation processes of solid samples. *Spectrochim. Acta B*, **45**, 1353–1367.

Kalsoom, U.I., Bashir, S., Ali, N., Akram, M., Mahmood, K. & Ahmad, R. (2012). Effect of ambient environment on excimer

laser induced micro and nano-structuring of stainless steel. *Appl. Surf. Sci*., **261**, 101–109.

Kaufman, V. & Martin, W.C. (1990). *Wavelength and Energy Level Classification of Magnesium Spectra for all Stages of Ionization (Mg I through Mg XII)*. Gaithersburg: National Institute of Standards and Technology.

Khalfaoui, W., Valerio, E., Masse, J.E. & Autric, M. (2010). Excimer laser treatment of ZE41 magnesium alloy for corrosion resistance and micro hardness improvement. *Opt. Lasers. Eng.*, **48**, 926–931.

Khan, S., Bashir, S., Hayat, A. & Khaleeq-ur-Rahman, M. (2013). Laser-induced breakdown spectroscopy of tantalum plasma. *Phys. Plasmas*, **20**, 073104.

Körner, C., Mayerhofer, R., Hartmann, M. & Bergmann, H.W. (1996). Physical and material aspects in using visible laser pulses of nanosecond duration for ablation. *J. Appl. Phys. A*, **63**, 123–131.

Legnaioli, S., Lorenzetti, G., Pardini, L., Cavalcanti, G.H. & Palleschi, V. (2014). *Applications of LIBS to the Analysis of Metals*. Heidelberg: Springer-Verlag.

Liu, Y., Jiang, M.Q., Yang, G.W., Guan, Y.J. & Dai, L.H. (2011). Surface rippling on bulk metallic glass under nanosecond pulse laser ablation. *Appl. Phys. Lett*., **99**, 91902.

Lacroix, D., Jeandel, G. & Boudot, C. (1997). Spectroscopic characterization of laser-induced plasma created during welding with a pulsed Nd: YAG laser. *J. Appl. Phys*., **81**, 6599–6606.

Majumdar, J.D., Galun, R., Mordike, B. & Manna, I. (2003). Effect of laser surface melting on corrosion and wear resistance of a commercial magnesium alloy. *Mater. Sci. Eng. A*, **361**, 119–129.

Mondal, A.K., Kumar, S., Blawert, C. & Dahotre, N.B. (2008). Effect of laser surface treatment on corrosion and wear resistance of ACM 720 Mg alloy. *Surf. Coat. Technol*., **202**, 3187–3198.

Moros, J., Fortes, F.J., Vadillo, J.M. & Laserna, J.J. (2014). *LIBS Detection of Explosives in Traces*. Heidelberg: Springer-Verlag.

Nakimana, A., Tao, H., Camino, A., Gao, X., Hao, Z. & Lin, J. (2012). Effect of ambient pressure on femtosecond laserinduced breakdown spectroscopy of Al in Argon. Presented at the *International Conference on Optoelectronics and Microelectronics (ICOM)*, pp. 146–150. Changchun, Jilin: IEEE.

Phipps, C. (2007). *Laser Ablation and Its Applications*. New York: Springer Science.

Reader, J., Corliss, C.H., Wiese, W.L. & Martin, G.A. (1980). *Wavelengths and Transition Probabilities for Atoms and Atomic Ions*. Washington DC: Center for Radiation Research, National Measurement Laboratory, National Bureau of Standards.

Salik, M., Hanif, M., Wang, J. & Zhang, X.Q. (2014). Spectroscopic characterization of laser-ablated manganese sulfate plasma. *Laser Part. Beams*, **32**, 137–144.

Shaheen, M.E., Gagnon, J.E. & Fryer, B.J. (2013). Femtosecond laser ablation of brass in air and liquid media. *J. Appl. Phys*. **113**, 213106.

Shaikh, N.M., Hafeez, S. & Baig, M.A. (2007). Comparison of zinc and cadmium plasma parameters produced by laser-ablation. *Spectrochim. Acta B*, **62**, 1311–1320.

Shaikh, N.M., Rashid, B., Hafeez, S., Jamil, Y. & Baig, M.A. (2006). Measurement of electron density and temperature of a laser-induced zinc plasma. *J. Phys. D: Appl. Phys*., **39**, 1384–1391.

Sabbaghzadeh, J., Dadras, S. & Torkamany, M. (2007). Comparison of pulsed Nd: YAG laser welding qualitative features with plasma plume thermal characteristics. *J. Phys. D: Appl. Phys*., **40**, 1047.

Warcholinski, B. & Gilewicz, A. (2009). Tribological properties of CrNx coatings. *J. Achiev. Mater. Manuf. Eng*., **37**, 498–504.

Weyl, G. M. (1989). Physics of laser-induced breakdown. In *Laser-induced plasmas and applications* (Dekker, M., ed.), pp. 1–59. New York: CRC Press.

Yousaf, D., Bashir, S., Akram, M., kalsoom, U.I. & Ali, N. (2013). Laser irradiation effects on the surface, structural and mechanical properties of Al–Cu alloy 2024. *Radiat. Eff. Defects*, **169**, 144–156.

Yu, J.J. & Lu, Y.F. (1999). Laser-induced ripple structures on Ni–P substrates. *Appl. Surf. Sci*., **148**, 248–252.